GOMsphere: A Comprehensive Geometrical Optics FORTRAN Code for Computation of Absorption and Single Scattering Properties of Large Dielectric Spheres – Documentation of Algorithm (Version 1.0, May 2003)

Xiaobing Zhou (xzhou@nmt.edu)

Department of Earth and Environmental Science
New Mexico Institute of Mining and Technology
801 Leroy Place, Socorro, NM 87801

Shusun Li (sli@asf.alaska.edu)

Geophysical Institute, University of Alaska Fairbanks
P.O.Box 757320, Fairbanks, AK 99775-7320
Email: sli@asf.alaska.edu

Knut Stamnes (kstamnes@stevens-tech.edu)

Light and Life Laboratory
Department of Physics and Engineering Physics
Stevens Institute of Technology
Castle Point on Hudson Hoboken, NJ 07030

ABSTRACT. Absorption of solar radiation by snow grains in the near-infrared part of the solar spectrum can not be neglected when computing radiative properties of snow. Thus, a geometrical optics method is developed to compute scattering and absorption cross section of particles of arbitrary complex refractive index assuming large snow meltclusters (1 cm-order), observed ubiquitously in the snow cover during summer, can be characterized as spheres, one may compute absorption and scattering efficiencies, and the scattering phase function on the basis of this geometrical optics method. The number of internal reflections and transmissions are truncated based on the ratio of incident irradiance at the n-th interface to the initial incident irradiance within a specific optical ray. Phase functions for both near- and far-field are directly calculated at a specific scattering angle using a hybrid algorithm based on the bisection and Newton-Raphson methods. With these methods the absorption and scattering properties of a single particle can be calculated for any wavelength in the solar spectrum or microwave region. This “Geometrical Optics Method for SPHEREs” code (GOMsphere) is tested against Wiscombe’s Mie scattering code (MIE0) for a range of size parameters. It can be combined with MIE0 to calculate the single scattering properties of snow grains of any size.

1. Introduction

To model the surface reflectance of snow cover using radiative transfer, we need basic optical properties of individual snow grains. For small spherical particles such as water cloud, the optical properties can be computed exactly from Mie theory [Wiscombe, 1979; 1980] and parameterized as a function of liquid water path and grain size [Hu and Stamnes, 1993]. For non-spherical particles, unlike the spherical case, where the exact Mie theory is available, no benchmarked computational techniques are generally available, although research on light scattering by non-spherical particles is being actively pursued [Liou and Takano, 1994; Mishchenko et al., 1996; Rother and Schmidt, 1996; Mishchenko, 2000]. Grains in wet snow or liquid-saturated snow (liquid water content, LWC, ≥7%) tend to be cohesionless spherical particles [Colbeck, 1979]. Thus, single scattering properties of snow grains can be obtained using Mie scattering theory [Wiscombe, 1979; 1980; van de Hulst, 1957; Bohren and Huffman, 1983]. However, for moist or low liquid content (<7%) snow, grains tend to form multigrain clusters. Clusters of grains are widely observed in snow covers [Bager, 1962; Sturm et al., 1998; Massom, et al., 1998]. Due to frequent melt-refreezing cycles, summer snow cover on Antarctic sea ice is characterized by ubiquitous icy clusters, ice lenses, ice layers, and percolation columns, with grain size of 1 cm-order [Hass, 2001; Morris and Jeffries, 2001; Massom et al., 2001]. Centimeter-scale icy nodules in snow were also observed in winter, after a surface thaw-freeze event [Massom et al., 1997; 1998]. It has been found that the albedo is correlated with snow composite grain size of 1 cm-order instead of the single grains of 1 mm-order that make up composite grains [Zhou, 2002]. This indicated that composite grains such as meltclusters may play an important role in the radiative properties of summer snow cover. Retrieval algorithms based on the comparison between measured radiance or reflectance data from satellite sensors and those obtained from radiative transfer modeling need the scattering properties of the target particles [Nakajima and Nakajima, 1995]. To understand the interaction of electromagnetic radiation with snow grains and its role in the remote sensing of snow cover, it is imperative to obtain the

single scattering properties of the composite grains ubiquitously observed in summer snow cover.

In principle, the single scattering properties can be calculated using Mie theory for spheres of any size. But the Mie solutions are expansions on the size parameter $x = 2\pi a/\lambda$, where a is the radius of spherical scatterers and λ is the wavelength of the incident radiation. Numerous complex terms are needed for the general solutions for large values of x [Kokhanovsky and Nakajima, 1998]. For this reason, available Mie codes can be used for $x < 20000$. For large values of x, the best method is the ray optics approximation [van de Hulst, 1957; Nussenzveig, 1992]. In the framework of this approach, the scattering characteristics are represented as expansions with the parameter λ/a, so that only a few terms should be calculated to obtain a converged solution. The geometrical optics method has been extensively used in scattering of radiation not only from spherical particles [van de Hulst, 1957], but also from non-spherical particles [Nakajima et al., 1998]. Calculation from a Monte Carlo code based on the geometrical optics method shows that differences in simulated radiances between the GOM and the Mie calculation decrease as the size parameter increases even when the magnitude of the two phase functions at the scattering angle are almost the same [Nakajima et al., 1998]. It is expected that results from the geometrical optics approach will converge to those of Mie theory when the size/wavelength ratio becomes sufficiently large [van de Hulst, 1957].

The purpose of this document is to summarize the development of a practical and fast code (GOMsphere) using a geometrical optics method for calculation of absorption coefficients, scattering coefficients and phase functions for both near- and far-field absorption and scattering of solar radiation by grains within a snow cover. For simplicity, the shape of snowmelt clusters or composite grains is characterized as spherical. There are two main reasons that justify this simplification. First, it is questionable to adopt one particular shape as representative for snow grains in snow cover. Besides, with time evolution, metamorphism makes all kinds of snow grains round off. Second, Grenfell and Warren (1999) found that a nonspherical ice particle can be represented by a collection of independent spheres that has the same volume-to-surface-area ratio as the nonspherical

particle, based on a finding by Hansen and Travis (1974) that dispersive media with different particle size distributions but the same values of the effective radius have approximately the same light scattering and absorption characteristics. For the complex refractive index $\hat{m}$ of snow and ice, data are primarily taken from the updated compilation by Warren (1984). Measurements by Kou et al. (1993) of the imaginary part of the complex refractive index for polycrystalline ice in the 1.45-2.50-μm region agree well with Warren's compilation. Discrepancies between the two data sets in this spectral region occur mainly near 1.50-, 1.85- and 2.50-μm, with the largest discrepancy near 1.85-μm. Gaps in the data at ultraviolet wavelengths in the 0.25- to 0.40-μm region were filled by Perovich and Govoni (1991). The temperature dependence of the refractive index of ice for λ<100 μm is deemed to be negligible for most temperatures that would be found on Earth [Warren, 1984a]. With the spectral complex refractive index available, the spectral dependence of the optical properties of a single snow grain can be calculated using GOMsphere.

2. Radiative Transfer Equations and Single Scattering Properties

The general equation for radiation at wavelength λ in a dispersive medium may be written as

$$\cos\theta \frac{d\mathrm{I}_\lambda(\tau,\theta,\varphi)}{d\tau} = -\mathrm{I}_\lambda(\tau,\theta,\varphi) + \frac{\omega_0}{4\pi}\int_0^{2\pi} d\varphi' \int_0^{\pi} d\theta' P(\tau;\theta,\varphi;\theta',\varphi')\mathrm{I}_\lambda(\theta',\varphi')\sin\theta' + S_{\lambda,extn}(\theta,\varphi) \quad (1)$$

where $\mathrm{I}_\lambda(\tau,\theta,\varphi)$ is the radiance, τ is the optical depth [Kokhanovsky, 1999; Thomas and Stamnes, 1999]. $S_{\lambda,extn}(\theta,\varphi)$ is the external source such as blackbody emission or the solar pseudo-source.

$$P(\tau;\mu,\varphi;\mu',\varphi') = \frac{4\pi C_{sca}^d(\tau;\mu,\varphi;\mu',\varphi')}{C_{sca}} = \frac{4\pi C_{sca}^d(\tau,\Theta)}{C_{sca}}$$

is the phase function. $\mu = \cos\theta$. C_{sca}^d is the differential scattering cross-section. For isotropic media, the value of $C_{sca}^d(\tau;\mu,\varphi;\mu',\varphi')$ depends only on the scattering angle Θ:

$\Theta = \arccos\left(\mu\mu' + \sqrt{1-\mu^2}\sqrt{1-\mu'^2}\cos(\varphi-\varphi')\right)$, thus $C_{sca}^d(\tau;\mu,\varphi;\mu',\varphi') = C_{sca}^d(\tau,\Theta)$. The physical meaning of $P(\tau;\mu,\varphi;\mu',\varphi')$ is that it is the probability of a photon scattering from the direction $\Omega' = (\theta',\varphi')$ to the direction $\Omega = (\theta,\varphi)$. $C_{sca} = C_{ext} - C_{abs}$ is the total scattering cross section:

$$C_{sca} = 2\pi\int_0^\pi d\Theta C_{sca}^d(\tau,\Theta)\sin\Theta$$

The total extinction coefficient σ_{ext} and the absorption coefficient σ_{abs} depend on the number concentration of particles *n* and their absorption cross-section C_{abs} and scattering cross-section C_{sca} [Bohren and Barkstrom, 1974; Thomas and Stamnes, 1999; Kokhanovsky, 1999]

$$\sigma_{ext} = nC_{ext}, \quad \sigma_{sca} = nC_{sca}, \quad \sigma_{abs} = nC_{abs}, \quad C_{ext} = C_{sca} + C_{abs} \tag{2a}$$

where C_{ext} is the extinction cross-section.

$$\omega_0 \equiv \sigma_{sca}/\sigma_{ext} = \sigma_{sca}/(\sigma_{abs}+\sigma_{sca}) = C_{sca}/C_{ext} = Q_{sca}/Q_{ext} \tag{2b}$$

is the single-scattering albedo. $Q_{sca} = C_{sca}/\pi a^2$ and $Q_{ext} = C_{ext}/\pi a^2$ are scattering efficiency and extinction efficiency, respectively. The phase function is thus expressed in terms of the scattering cross section and differential scattering cross-section

$$P(\tau;\mu,\varphi;\mu',\varphi') = \frac{4\pi C_{sca}^d(\tau,\Theta)}{C_{sca}} = \frac{2C_{sca}^d(\tau,\Theta)}{\int_0^\pi d\Theta C_{sca}^d(\tau,\Theta)\sin\Theta} \tag{3}$$

Obviously, the phase function satisfies the normalization function

$$\frac{1}{4\pi}\int P(\tau;\Theta,\Psi)d\Omega = 1,$$

where $d\Omega = \sin\Theta d\Theta d\Psi$ is the element of solid angle. Based on the phase function, the asymmetry factor is defined as

$$g = \langle\cos\Theta\rangle = \frac{1}{4\pi}\int P(\tau;\Theta,\Psi)\cos\Theta d\Omega \tag{4}$$

3. Single Scattering Properties -- Formalism

Scattering by a particle is actually the sum of the reflection and refraction plus the Fraunhofer diffraction. Reflection and refraction make the outgoing (scattered) light distributed in all directions dependent on the optical properties of the particles. The diffraction pattern is more or less a narrow and intense lobe around the forward scattering direction, $\Theta = 0°$. Diffraction depends on the form and size of the particle but is independent of the optical properties of the particle, and is thus a purely geometric effect.

The general forms of the electromagnetic field $(\mathbf{E}, \mathbf{H})$ plane electromagnetic waves, which is a solution of the Maxwell equations, are

$$\mathbf{E} = \mathbf{E_0} e^{i(\mathbf{k}\cdot\mathbf{x}-\omega t)} \tag{5}$$

where $\mathbf{k} = k\hat{e}$ is the complex wave vector ($\hat{e}$ is a unit vector in the propagation direction), and the wave propagates along space vector **x**. The wave frequency is ω and t is time. The wave number k is

$$k = \frac{\omega \hat{m}}{c} = \frac{2\pi \hat{m}}{\lambda} = \omega\sqrt{\varepsilon\mu} = \frac{2\pi m'}{\lambda} + i\frac{2\pi m''}{\lambda} \tag{6}$$

where $\hat{m}$ is the complex refractive index of snow. Inserting Equation (6) into Equation (5), the electric field takes the form

$$\mathbf{E} = \mathbf{E_0} e^{-\frac{2\pi m''}{\lambda} z} e^{i\left(\frac{2\pi m'}{\lambda} z - \omega t\right)} = \mathbf{E_0} e^{-\gamma_1 z} e^{i(\gamma_2 z - \omega t)}, \quad \gamma_1 = \frac{2\pi m''}{\lambda}, \quad \gamma_2 = \frac{2\pi m'}{\lambda} \tag{7}$$

where γ_1 and γ_2 are absorption constant and phase constant, respectively [Hallikainen and Winebrenner, 1992]. $z = \hat{e}\cdot\mathbf{x}$. λ is the wavelength and ω the angular frequency of the incident electromagnetic (EM) wave, c the speed of light *in vacuo*, ε the complex permittivity and μ the permeability of the medium. Radiative transfer processes of electromagnetic waves (radiation) by snow are simplified as the scattering and absorption of plane waves by snow grains. The Poynting vector of a plane wave is

$$\mathbf{S} = \frac{1}{2}\mathrm{Re}\left\{\mathbf{E}\times\mathbf{H}^*\right\} = F_\lambda \hat{\mathbf{e}} \tag{8}$$

where

$$F_\lambda = \frac{1}{2}\mathrm{Re}\left\{\sqrt{\frac{\varepsilon}{\mu}}\right\}\left|\mathbf{E}_0\right|^2 \exp\left(-\frac{4\pi m'' z}{\lambda}\right)$$
$$= \frac{m'}{2Z_0}\left|\mathbf{E}_0\right|^2 \exp(-\beta z), \qquad \beta = \frac{4\pi m''}{\lambda} = 2\gamma_1, Z_0 = \sqrt{\mu_0/\varepsilon_0}$$

where F_λ is the amplitude of the Poynting vector (it is also called the spectral irradiance or energy flux at wavelength λ). Z_0 is the impedance of free space, its dimensions are energy per unit area, time and wavelength. β is the absorption coefficient. Note that for energy flux, the attenuation constant due to absorption is called the absorption coefficient, while for the EM field, it is called the absorption constant.

3.1 Truncation of the Number of Rays Emerging from a Sphere

Each snow particle is assumed to be internally homogeneous and axisymmetric, and is assumed to reside in air. For a snow grain whose radius is much larger than the wavelength of the incident wave, we adopt the ray tracing method to calculate the single scattering properties [van de Hulst, 1957; Bohren and Huffman, 1983]. Supposing the incident wave is p-polarized, p = // or ⊥ indicates that the wave is parallel- or perpendicular-polarized. Reflection and transmission occurs only at an interface between media with different indices of refraction. Figure 1 illustrates absorption and scattering by a spherical snow grain in the geometrical optics picture. The initial ray separates into reflected and refracted sub-rays after it hits the particle surface. Energy contained in each ray decreases rapidly as it propagates by reflection and refraction. The thickness of the arrowed lines denote this debasement of energy in each ray. All rays emerging from the central grain will participate in the same process with the other grains, resulting in multiple scattering. Here, we concentrate only on the single-scattering properties of snow grains. With full knowledge of single-scattering properties, multiple scattering can be treated using radiative transfer theory [c.f. Zhou, 2002]. At the jth interface, which is defined as the order of interface between the particle and the incident light ray, assuming the incident electric field is $E^j_{p,i}$, the reflected ($E^j_{p,r}$) and transmitted ($E^j_{p,t}$) electric fields are [Hecht, 1998]

$$E_{p,r}^{j} = r_p^{j} E_{p,i}^{j}, \qquad E_{p,t}^{j} = t_p^{j} E_{p,i}^{j} \tag{9}$$

where

$$r_p^{j} = r_p\left(\Theta_i, \Theta_t, \hat{m}\right) = r_p, \qquad t_p^{j} = t_p\left(\Theta_i, \Theta_t, \hat{m}\right) = t_p, \qquad j = 1$$
$$r_p^{j} = r_p\left(\Theta_t, \Theta_i, 1/\hat{m}\right), \qquad t_p^{j} = t_p\left(\Theta_t, \Theta_i, 1/\hat{m}\right), \qquad j > 1$$

The reflection coefficients r_p and transmission coefficients t_p are complex and complicated for absorbing and scattering media. Following the discussion for wave reflection and transmission of metallic film of Born and Wolf (1980) (p.628-631), and setting $\hat{m}\cos\Theta_t = u + iv, (i = \sqrt{-1})$, r_p and t_p take the following form (see Appendix A)

$$\begin{cases} r_{//}\left(\Theta_i, \Theta_t, \hat{m}\right) = \dfrac{\left[\left(m'^2 - m''^2\right)\cos\Theta_i - u\right] + i\left(2m'm''\cos\Theta_i - v\right)}{\left[\left(m'^2 - m''^2\right)\cos\Theta_i + u\right] + i\left(2m'm''\cos\Theta_i + v\right)} \\ t_{//}\left(\Theta_i, \Theta_t, \hat{m}\right) = \dfrac{2\left(m' + im''\right)\cos\Theta_i}{\left[\left(m'^2 - m''^2\right)\cos\Theta_i + u\right] + i\left(2m'm''\cos\Theta_i + v\right)} \end{cases} \tag{10a}$$

$$\begin{cases} r_{\perp}\left(\Theta_i, \Theta_t, \hat{m}\right) = \dfrac{\left(\cos\Theta_i - u\right) - iv}{\left(\cos\Theta_i + u\right) + iv} \\ t_{\perp}\left(\Theta_i, \Theta_t, \hat{m}\right) = \dfrac{2\cos\Theta_i}{\left(\cos\Theta_i + u\right) + iv} \end{cases} \tag{10b}$$

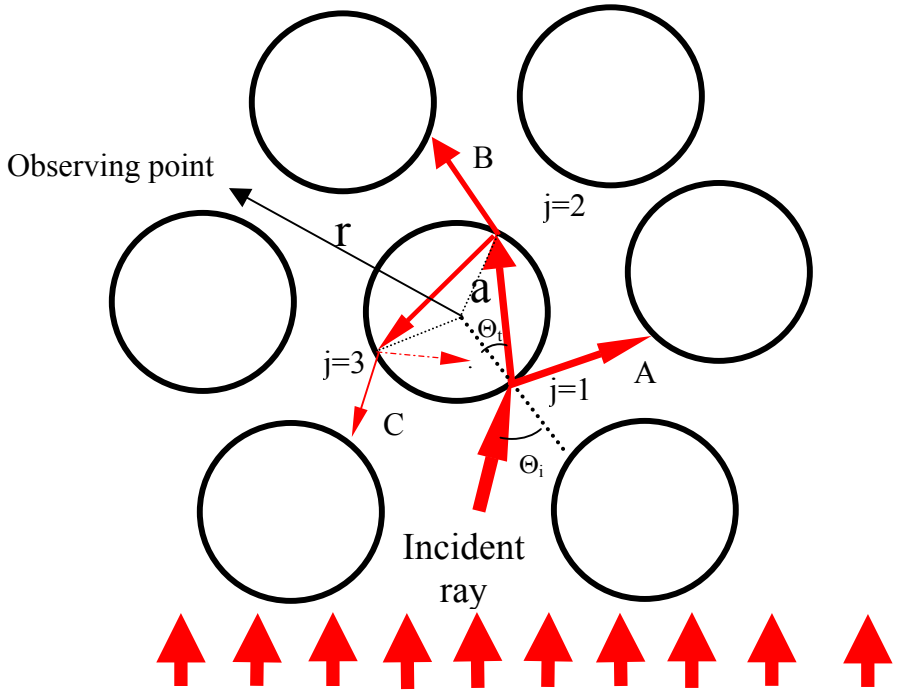

and

$$\begin{cases} r_p\left(\Theta_t,\Theta_i,1/\hat{m}\right) = -r_p\left(\Theta_i,\Theta_t,\hat{m}\right) \\ t_p\left(\Theta_t,\Theta_i,1/\hat{m}\right) = \dfrac{(u+iv)}{\cos\Theta_i} t_p\left(\Theta_i,\Theta_t,\hat{m}\right) \end{cases} \tag{10c}$$

with

$$\begin{cases} u = \dfrac{\sqrt{2}}{2}\left\{\left[\left(m'^2 - m''^2 - \sin^2\Theta_i\right)^2 + 4m'^2 m''^2\right]^{\frac{1}{2}} + \left(m'^2 - m''^2 - \sin^2\Theta_i\right)\right\}^{\frac{1}{2}} \\ v = \dfrac{\sqrt{2}}{2}\left\{\left[\left(m'^2 - m''^2 - \sin^2\Theta_i\right)^2 + 4m'^2 m''^2\right]^{\frac{1}{2}} - \left(m'^2 - m''^2 - \sin^2\Theta_i\right)\right\}^{\frac{1}{2}} \end{cases}$$

where Θ_i is the incident angle(real), Θ_t is the refraction angle (complex).

Between two consecutive interfaces, the ray travels a path length of

$$\begin{aligned} \xi &= \left|2a\cos\Theta_t\right| \\ &= \frac{2a}{m'^2 + m''^2}\sqrt{\left(um' + vm''\right)^2 + \left(vm' - um''\right)^2} \end{aligned}$$

where a is the radius of the spherical snow grain. The incident electric field at the jth interface ($j \geq 2$) is related to the reflected electric field at the (j-1)th interface ($j > 2$) or transmitted field when j = 2 by the following relations

$$\begin{aligned} E_{p,i}^j &= e^{-\gamma_1\xi} E_{p,t}^{j-1} = e^{-\beta\xi/2} E_{p,t}^{j-1}, \qquad j = 2 \\ E_{p,i}^j &= e^{-\gamma_1\xi} E_{p,r}^{j-1} = e^{-\beta\xi/2} E_{p,r}^{j-1}, \qquad j > 2 \end{aligned}$$

At the jth interface,

$$\begin{aligned} E_{p,i}^j &= \begin{cases} E_{p,i}, & j = 1 \\ t_p \prod_{l=2}^{j}\left(r_p^l\right) e^{-\beta\xi(j-1)/2} E_{p,i} = t_p\left(-r_p\right)^{j-2} e^{-\beta\xi(j-1)/2} E_{p,i}, & j \geq 2 \end{cases} \\ E_{p,t}^j &= \begin{cases} t_p E_{p,i}, & j = 1 \\ t_p^j E_{p,i}^j = \dfrac{(u+iv)}{\cos\Theta_i}\left(t_p\right)^2\left(-r_p\right)^{j-2} e^{-\beta\xi(j-1)/2} E_{p,i}, & j \geq 2 \end{cases} \\ E_{p,r}^j &= \begin{cases} r_p E_{p,i}, & j = 1 \\ r_p^j E_{p,i}^j = t_p\left(-r_p\right)^{j-1} e^{-\beta\xi(j-1)/2} E_{p,i}, & j \geq 2 \end{cases} \end{aligned} \tag{11}$$

Rays emerging from the surface of the sphere are called scattered rays. They include reflected and transmitted rays. From Equation (11), we obtain the scattered field near the surface of the sphere (near field, r = a)

$$E_{p,s}^{j} = \varepsilon_p^j E_{p,i}, \qquad \varepsilon_p^j = \begin{cases} r_p, & j = 1 \\ \dfrac{(u+iv)}{\cos\Theta_i}(t_p)^2(-r_p)^{j-2} e^{-\beta\xi(j-1)/2}, & j \geq 2 \end{cases} \tag{12}$$

The rays reflected from the first interface is the only reflected radiation and the other rays are transmitted radiation. The angle of the emergent ray at the jth interface from the sphere that deviates from the incident direction is [van de Hulst, 1957; Glantschnig and Chen, 1981]

$$\Theta'(j,\Theta_i) = 2(j-1)|\Theta_t| - 2\Theta_i - (j-2)\pi, \qquad j = 1,2,... \tag{13a}$$

which defines the scattering angle Θ in the interval (0, π) by

$$\Theta' = l \cdot 2\pi + q\Theta \tag{13b}$$

where l is an integer and $q = \pm 1$. The complex refraction angle Θ_t is obtained from the law of refraction as

$$\begin{aligned} \Theta_t &= \sin^{-1}\left[\frac{(m'-im'')\sin\Theta_i}{m'^2+m''^2}\right] \\ &= -i\ln\left\{i\frac{(m'-im'')\sin\Theta_i}{m'^2+m''^2} + \sqrt{1-\left[\frac{(m'-im'')\sin\Theta_i}{m'^2+m''^2}\right]^2}\right\} \end{aligned} \tag{14}$$

where the other root of inverse sine function of complex argument in obtaining Θ_t is discarded based on the physical refraction process. For any incident ray, l is the nearest integer of $\dfrac{\Theta'}{2\pi}$ and $fra\left(\dfrac{\Theta'}{2\pi}\right)$ is the remainder of $\dfrac{\Theta'}{2\pi}$, i.e.

$$l = \begin{cases} \text{int}\left(\dfrac{\Theta'}{2\pi} + 0.5\right) & if\ \dfrac{\Theta'}{2\pi} \geq 0 \\ \text{int}\left(\dfrac{\Theta'}{2\pi} - 0.5\right) & if\ \dfrac{\Theta'}{2\pi} < 0 \end{cases} \tag{15a}$$

with int(a) = 0 if |a| < 1, or int(a) = the integer part of a, disregarding the fractional part if |a| > 1. $fra\left(\frac{\Theta'}{2\pi}\right)$ can be expressed as

$$fra\left(\frac{\Theta'}{2\pi}\right) = \frac{\Theta'}{2\pi} - l$$

from which we have

$$q = \begin{cases} +1, & if \quad fra\left(\frac{\Theta'}{2\pi}\right) > 0 \\ -1, & if \quad fra\left(\frac{\Theta'}{2\pi}\right) \le 0 \end{cases} \tag{15b}$$

This way, the scattering angle for each ray emerging from the sphere is determined. The monotonical relationships between the scattering angle (Θ) and the incident angle (Θ_i) at the first five interfaces (j = 1, 2, …, 5) for λ = 0.5 μm are shown in Figure 2. At a specific interface for any incident angle, the scattering angle of the ray is independent of the size of the ice sphere.

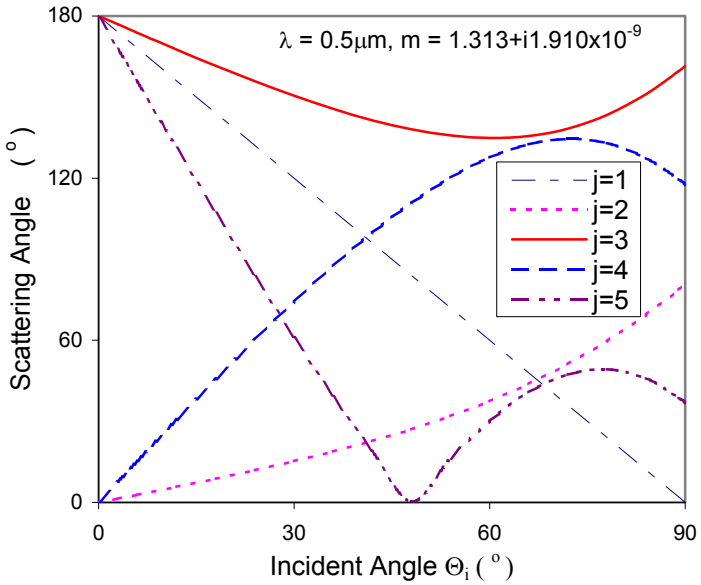

Figure 2 Relationship between outgoing angle Θ at a specific interface j and incident angle Θ_i. The five curves correspond to the first five interfaces once a light ray enters an ice sphere. The wavelength for each case is λ = 0.5 μm and refractive index m = 1.313+i1.910×10^{-9}.

Differentiation of Θ' and Θ with respect to Θ_i by use of Snell's law yields

$$\frac{d\Theta}{d\Theta_i} = q\frac{d\Theta'}{d\Theta_i} = 2q\left[(j-1)\left|\frac{\cos\Theta_i}{u+iv}\right| - 1\right] \tag{16}$$

Inserting Equation (10) into Equation (8), we can obtain the incident, transmitted or reflected irradiances at the jth interface. The irradiance absorbed between the (j-1)th and jth interfaces is

$$F_{j-1,j}(\Theta_i, m) = \left|t_p\right|^2 \left(R_p\right)^{j-2} e^{-\beta\xi(j-2)}\left(1 - e^{-\beta\xi}\right) m' F_0 \tag{17}$$

where $F_0 = \dfrac{1}{2Z_0}\left|E_{p,i}\right|^2$ is the incident irradiance on the sphere.

Assume the incident radiation is unpolarized, the total absorbed energy (summed over all ray paths and integrated over the sphere surface for all incident angles) is then [Bohren and Huffman, 1983]

$$\begin{aligned} W_{abs} &= \int_0^{\pi/2}\int_0^{2\pi} \sum_{j=2}^{N} F_{j-1,j}(\Theta_i, m)\left|\cos\Theta_t\right| a^2 \sin\Theta_i d\Theta_i d\Psi_i \\ &= 2\pi a^2 F_0 \int_0^1 T(\mu_i)\sum_{j=2}^{N}\left(\mathrm{Re}^{-\beta\xi}\right)^{j-2}\left(1 - e^{-\beta\xi}\right)\mu_i d\mu_i \end{aligned} \tag{18}$$

where

$$\begin{aligned} T &= \frac{1}{2}\left(T_{//} + T_{\perp}\right), \quad with \quad T_p = \frac{m'\sqrt{\left(um'+vm''\right)^2 + \left(vm'-um''\right)^2}}{\left(m'^2+m''^2\right)\cos\Theta_i}\left|t_p\right|^2 \\ R &= \frac{1}{2}\left(R_{//} + R_{\perp}\right), \quad with \quad R_p = \left|r_p\right|^2 \end{aligned} \tag{19}$$

where $\mu_i = \cos\Theta_i$, R is the reflectance and T is the transmittance. For spherical particles with arbitrary absorption coefficient, sum over the interface number is, theoretically, to infinite. However, based on the strength of the incident electric field at the jth interface, the series can be truncated at some value, for instance N, at which interface the electric field is so weak compared with the incident field that further calculation does not make any difference. Supposing the truncation is made when the ratio of the irradiance or energy flux at the jth interface to that incident at the first interface (j = 1) is equal to some

small tolerance number ς, we can obtain the maximum number N of interfaces to be summed over in Equation (18). Supposing

$$R = |r|^2,\ T = \frac{m'\sqrt{(um'+vm'')^2 + (vm'-um'')^2}}{(m'^2+m''^2)\cos\Theta_i}|t|^2,$$

where

$$t = \sqrt{0.5\left(t_{//}^{\ 2} + t_{\perp}^{\ 2}\right)}$$
$$r = \sqrt{0.5\left(r_{//}^{\ 2} + r_{\perp}^{\ 2}\right)}$$

and replacing r_p and t_p with r and t in Equation (11), and combining with Equation (8), N is found to be

$$N(\Theta_i) = \frac{\beta\xi + 2\ln|t| - 2\ln R - \ln\varsigma}{\beta\xi - \ln R} \tag{20}$$

Thus, summation over j in Equation (18) is from 2 to N. The relationship of N to incident angle for the case of green light $\lambda = 0.5$ μm is shown in Figure 3a for an ice sphere of radius a = 1 cm. The same calculation for $\lambda = 2.0$ μm shows that N = 2 for all incident angles. Glantschnig and Chen (1981) compared the angular scattering diagrams using the results from geometrical optics approximation with N = 2 for $\lambda = 0.49$ μm with the exact Mie calculation. They found that for $\Theta_i \leq 60°$, the agreement is reasonable, and at grazing or near grazing angles, the geometrical optics theory does not give good results. From Figure 3a, we can see that for the green light N increases rapidly with increasing incident angle when it is greater than about 80°. This illustrates that the approximation N = 2 is not enough for the calculation of light scattering by weak absorbing scatterers at large incident angles. The relationship of N with wavelength λ is shown in Figure 3b for Θ_i = 60°. For visible light, ice is very weakly absorbing, and attenuation is weaker so that a greater number of ray paths is needed, while for near infrared ice is strongly absorbing and only 1 or 2 paths are necessary to extinguish the transmitted radiation.

3.2 Absorption

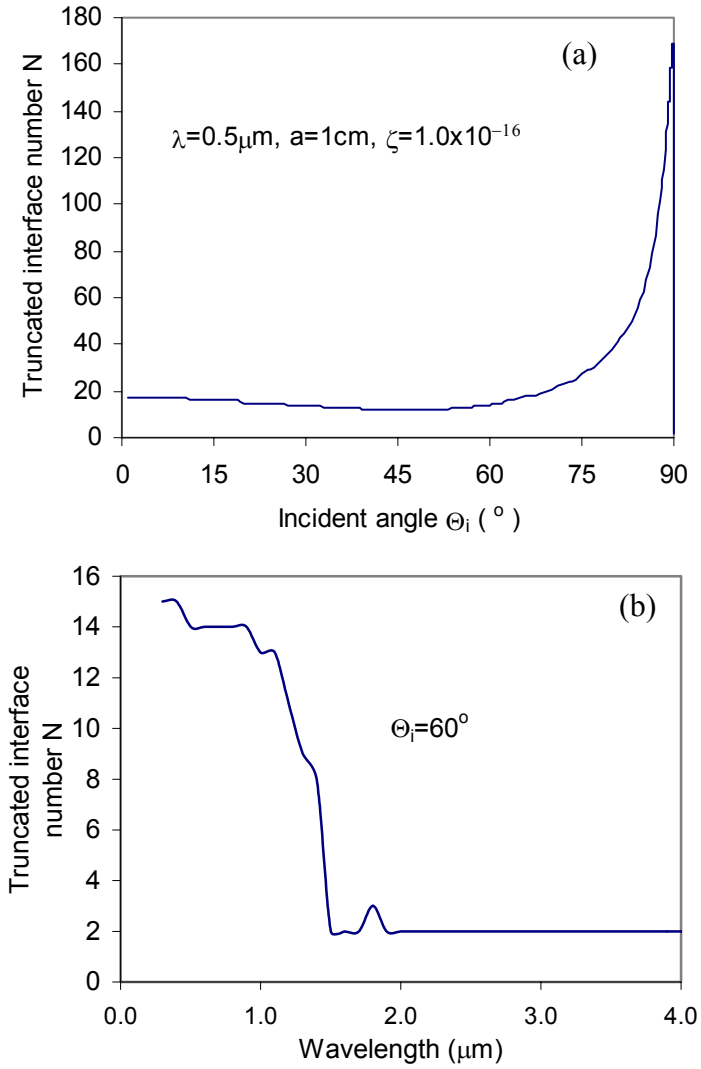

Figure 3 (a) Maximum number N versus incident angle for the truncation in the sum series of the calculation of absorption efficiency for an ice sphere with radius a = 1 cm and truncation tolerance $\varsigma = 1.0\text{x}10^{-16}$ for wavelength $\lambda = 0.5$ μm; and (b) the maximum number N versus wavelength λ for the truncation in the sum series of the calculation of absorption efficiency of an ice sphere with radius a = 1 cm and truncation tolerance $\varsigma = 1.0\text{x}10^{-16}$ for incidence angle $\Theta_i = 60°$.

From the total energy absorbed and the initial incident irradiance, the absorption cross-section and absorption efficiency are obtained as (N→∞)

$$C_{abs} = \frac{W_{abs}}{F_0} = 2\pi a^2 \int_0^1 T(\mu_i) \sum_{j=2}^{N} \left(\mathrm{Re}^{-\beta\xi}\right)^{j-2} \left(1 - e^{-\beta\xi}\right) \mu_i d\mu_i$$
$$= 2\pi a^2 \int_0^1 T(\mu_i) \frac{1 - \exp(-\beta\xi)}{1 - \mathrm{Re}\, xp(-\beta\xi)} \mu_i d\mu_i \tag{21a}$$

$$Q_{abs} = \frac{C_{abs}}{\pi a^2} = 2\int_0^1 T(\mu_i) \frac{1 - \exp(-\beta\xi)}{1 - \mathrm{Re}\, xp(-\beta\xi)} \mu_i d\mu_i \tag{21b}$$

The total energy scattered by a large sphere includes the diffracted, reflected, and transmitted components. Thus, the scattering cross-section of a large sphere can be written as [Bohren and Huffman, 1983]

$$C_{sca} = \frac{\sum_{j=1}^{N} W_{sca}^{j}}{F_0} = C_{dif} + C_{ref} + C_{tra} \tag{22}$$

3.3 Near-field Scattering

Scattered rays at the first interface are exclusively the reflected component. All emerging rays from the second interface on are included in the transmitted component. In the same manner as obtaining Equation (21), using Equation (8), Equation (12) and Equation (19), we can derive components of Equation (22) for unpolarized incident radiation as follows

$$C_{ref} = \frac{W_{sca}^{1}}{F_0} = 2\pi a^2 \int_0^1 R(\mu_i) \mu_i d\mu_i \tag{23a}$$

$$C_{tra} = \frac{\sum_{j=2}^{N} W_{sca}^{j}}{F_0} = \pi a^2 \sum_{j=2}^{N} \int_0^1 \left[T_{//}^2(\mu_i) R_{//}^{j-2}(\mu_i) + T_{\perp}^2(\mu_i) R_{\perp}^{j-2}(\mu_i)\right] e^{-\beta\xi(j-1)} \mu_i d\mu_i \tag{23b}$$

Equation (23a) has the same form as the case of a non-absorbing sphere [Bohren and Huffman, 1983]. For the near field, the diffraction is Fresnel diffraction. Fraunhofer

diffraction will occur when the viewing distance $r > a^2/\lambda$ [Hecht, 1998]. For the incident plane waves, we will neglect the Fresnel diffraction.

Considering the energy distribution of the scattered ray in the scattering direction (scattering angle), the irradiance of the scattered ray at the sphere surface from the jth interface is expressed as the following, which is expanded to absorbing medium from non-absorbing [van de Hulst, 1957; Glantschnig and Chen, 1981; Liou and Hansen, 1971]

$$F_p\left(j,\Theta_i,\Theta\right)=\frac{-F_0\left|\varepsilon_p^j\right|^2\cos\Theta_i a^2\sin\Theta_i d\Theta_i d\Psi}{a^2\sin\Theta d\Theta d\Psi}=F_0\left|\varepsilon_p^j\right|^2 D \tag{24}$$

with

$$D\left(j,\Theta_i,\Theta\right)=\frac{\sin\left(2\Theta_i\right)}{4\left|\left(j-1\right)\dfrac{\cos\Theta_i}{\sqrt{u^2+v^2}}-1\right|\cdot\sin\Theta}$$

D is the geometrical divergence factor. Equation (16) and Snell's law have been used in deriving the above equation. Rainbows appear when $\frac{d\Theta}{d\Theta_i}=0$, under which $F_p\left(j,\Theta_i,\Theta\right)$ has a localized peak [Liou and Hansen, 1971]. This can be readily seen from Equation (24). In snow pack, a rainbow can be difficult to observe, but a localized peak exists at rainbow angles Θ_i^{rb}. For visible light, the imaginary part of the refractive index can be neglected, thus

$$\Theta_i^{rb}=\sin^{-1}\left(\sqrt{\frac{\left(j-1\right)^2-m'^2}{\left(j-1\right)^2-1}}\right).$$

For the general case,

$$\Theta_i^{rb}=\sin^{-1}\left\{\left[\frac{\left(j-1\right)^4-\left(m'^2-m''^2\right)-\left\{\left(j-1\right)^4\left[\left(m'^2+m''^2\right)^2-2\left(m'^2-m''^2\right)+1\right]-4m'^2m''^2\right\}^{1/2}}{\left(j-1\right)^4-1}\right]^{1/2}\right\}$$

Table 1 shows the rainbow angles for a spherical snow grain at any interface for 7 visible channels from blue to red (0.4-0.7 μm). Rainbow angle-widths Δ, which is defined as the

scattering angle difference between λ = 0.4 μm and λ = 0.7 μm for any of the rainbow series, are also shown. Most scattered energy is contained in the j = 1 to 4 components [Liou and Hansen, 1971]. Thus primary (j = 3) and secondary (j = 4) rainbows are the most important power peaks. The angle difference between the primary and secondary rainbows versus wavelength is shown in Figure 4. At $\lambda \approx 0.52$ μm, the angle difference has a minimum, indicating the primary and secondary rainbows within snow are nearest at $\lambda \approx 0.52$ μm.

Table 1 Incident angles (Θ_i) and scattering angles (Θ) at which rainbows appear for each visible channel (λ) at the j-th interface. Primary and secondary, etc. rainbows correspond to j = 3, 4, etc. The angle-width (Δ) of each rainbow is also shown.

	j = 3		4		5		6	
λ (μm)	Θ_i(°)	Θ(°)	Θ_i(°)	Θ(°)	Θ_i(°)	Θ(°)	Θ_i (°)	Θ(°)
0.40	60.20	135.90	72.28	132.74	77.16	46.83	79.88	37.20
0.45	60.42	135.34	72.4	133.75	77.25	48.25	79.95	35.38
0.50	60.58	134.93	72.49	134.49	77.31	49.28	80.00	34.07
0.55	60.70	134.61	72.56	135.05	77.36	50.07	80.03	33.06
0.60	60.79	134.36	72.61	135.50	77.39	50.70	80.07	32.26
0.65	60.87	134.15	72.66	135.88	77.43	51.22	80.09	31.59
0.70	60.94	133.97	72.69	136.02	77.45	51.68	80.11	31.01
Δ		1.94		3.46		4.85		6.19

From scattering theory [van de Hulst, 1957], the scattered irradiance at a distance r from the scatterer center is associated with incident irradiance through the differential scattering cross section $C_p^d\left(j,\Theta_i,\Theta\right)$ by

$$F_p\left(j,\Theta_i,\Theta\right)=\frac{C_p^d\left(j,\Theta_i,\Theta\right)}{r^2}F_0$$

Comparing this with Equation (24), we have the differential scattering cross section at the surface of the sphere

$$C_p^d\left(j,\Theta_i,\Theta\right)=a^2\left|\varepsilon_p^j\right|^2 D\left(j,\Theta_i,\Theta\right) \tag{25}$$

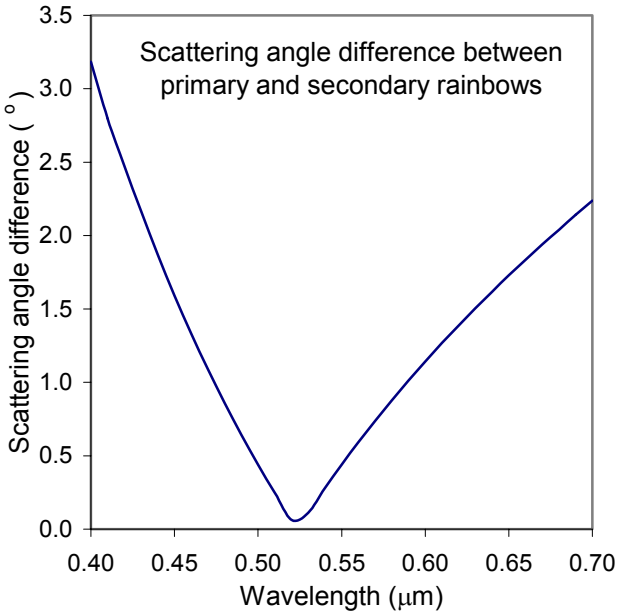

Figure 4 Scattering angle difference between primary and secondary rainbows versus wavelength. The primary and secondary rainbows are closest at $\lambda = 0.52$ μm.

For unpolarized natural light, the phase function (see Equation (3)) is thus

$$P^N(\Theta) = \frac{2\pi}{C_{sca}} \sum_{j,\Theta_i} \sum_p C_p^d(j, \Theta_i, \Theta) \tag{26a}$$

with

$$C_{sca}^N = \pi a^2 \int_0^\pi \sum_{j,\Theta_i} \left[\left| \varepsilon_{//}^j \right|^2 + \left| \varepsilon_\perp^j \right|^2 \right] D(j, \Theta_i, \Theta) \sin\Theta d\Theta \tag{26b}$$

and the asymmetry factor g^N for near-field scattering is (see. Equation (4)) [van de Hulst, 1957]

$$\begin{aligned} g^N &= \langle \cos\Theta \rangle \\ &= \frac{\pi}{C_{sca}} \int_0^\pi \sum_{j,\Theta_i} \sum_p C_p^d(j, \Theta_i, \Theta) \cos\Theta \sin\Theta d\Theta \end{aligned} \tag{26c}$$

$\sum_{j,\Theta_i}$ in Equation (26) is to sum over all sets of (j, Θ_i) that make up an emergent light ray with outgoing angle Θ. This guarantees that the irradiances of rays emerging at the same

scattering angle for a specific incident angle but from different interfaces, and those for a specific interface but from different incident angles, are added up. The extinction cross section is determined by

$$C_{ext}^{N} = C_{sca}^{N} + C_{abs} \tag{27}$$

Equations (22), (23), (26) and (27) constitute the main equations for near field scattering by large absorbing particles.

3.4 Far-field Scattering

For far-field scattering, the absorption is the same as expressed in Equation (21). Fraunhofer diffraction will be included in the calculation of scattering cross section. The irradiance of the scattered ray at the sphere surface from the jth interface is expressed as [van de Hulst, 1957; Glantschnig and Chen, 1981]

$$F_p\left(j,\Theta_i,\Theta\right) = \frac{F_0\left|\varepsilon_p^j\right|^2 \cos\Theta_i a^2 \sin\Theta_i d\Theta_i d\Psi}{r^2 \sin\Theta d\Theta d\Psi} = \frac{a^2}{r^2} F_0\left|\varepsilon_p^j\right|^2 D \tag{28}$$

From which the differential scattering cross section due to reflection and transmission $C_p^d\left(j,\Theta_i,\Theta\right)$ has the same form as Equation (25). Summing over all emerging rays from the same scattering angle we have the differential scattering cross section due to reflection and transmission for each incident light ray

$$C_p^d\left(\Theta_i,\Theta\right) = \sum_{j,\Theta_i} C_p^d\left(j,\Theta_i,\Theta\right) \tag{29}$$

The scattering cross section due to reflection and transmission of natural light is

$$\begin{aligned} C_{sca}^{rt} &= \int_{4\pi} C_p^d\left(\Theta_i,\Theta\right) d\Omega \\ &= \pi \int_0^{\pi} d\Theta \sin\Theta \sum_{j,\Theta_i} \sum_{p} C_p^d\left(j,\Theta_i,\Theta\right) \end{aligned} \tag{30}$$

Substituting Equation (29) and (30) into Equation (3), we obtain the phase function of scattering due to reflection and transmission for natural light and it has the same form as Equation (26a).

$$P^{rt}(\Theta_i,\Theta)=\frac{2\pi\sum_p C_p^d(\Theta_i,\Theta)}{C_{sca}}=\frac{2\pi}{C_{sca}}\sum_p\sum_{j,\Theta_i}C_p^d(j,\Theta_i,\Theta) \tag{31}$$

The asymmetry factor for this phase function is the same as Equation (26c)

Scattering amplitude functions expressed in terms of $C_p^d(j,\Theta_i,\Theta)$ are [van de Hulst, 1957; Glantschnig and Chen, 1981]

$$\left|S_p^{rt}(j,\Theta_i,\Theta)\right|=\sqrt{C_p^d(j,\Theta_i,\Theta)} \tag{32}$$

The scattering amplitude function due to Fraunhofer diffraction for both polarizations is given by Glantschnig and Chen (1981)

$$S_p^{dif}(\Theta)=x^2\left[\frac{J_1(x\sin\Theta)}{x\sin\Theta}\right],\qquad x=\frac{2\pi a}{\lambda} \tag{33}$$

where $J_1(x)$ is the first order Bessel function. From Equation (33) we have the differential cross section of Fraunhofer diffraction

$$C_p^{dif}(\Theta)=\left|S_p^{dif}(\Theta)\right|^2/k^2=a^2x^2\left[\frac{J_1(x\sin\Theta)}{x\sin\Theta}\right]^2=\frac{a^2J_1^2(x\sin\Theta)}{\sin^2\Theta} \tag{34}$$

The scattering cross section due to Fraunhofer diffraction is [van de Hulst, 1957]

$$C^{dif}=\int\frac{1}{2}\sum_p C_p^{dif}(\Theta)d\Omega=2\pi a^2\int_0^\pi\frac{J_1^2(x\sin\Theta)}{\sin\Theta}d\Theta=\pi a^2 \tag{35}$$

The phase function resulting from the Fraunhofer diffraction is (see Equation (3))

$$P^{dif}(\Theta)=\frac{4J_1^2(x\sin\Theta)}{\sin^2\Theta} \tag{36}$$

from which the asymmetry factor due to diffraction is derived as

$$g^{dif}=\frac{1}{4\pi}\iint P^{dif}(\Theta)\cos\Theta d\Omega=2\int_0^\pi J_1^2(x\sin\Theta)\cot(\Theta)d\Theta \tag{37}$$

Based on Equation (32) and Equation (33), the full scattering amplitude functions are calculated by

$$S_p(\Theta_i,\Theta)=S_p^{dif}(\Theta)+\sum_{j,\Theta_i}S_p^{rt}(j,\Theta_i,\Theta) \tag{38}$$

The total differential scattering cross section due to reflection, transmission and diffraction can be obtained from Equations (29) and (34)

$$\begin{aligned} C_{sca}^{d}(\Theta_i,\Theta) &= \frac{1}{2}\sum_{p}\left(C_p^{d}(\Theta_i,\Theta)+C_p^{dif}(\Theta)\right) \\ &= \frac{1}{2}\sum_{j,\Theta_i}\sum_{p} C_p^{d}(j,\Theta_i,\Theta)+\frac{a^2 J_1^2(x\sin\Theta)}{\sin^2\Theta} \end{aligned} \tag{39}$$

The phase function is easily obtained if we insert Equation (39) into Equation (3), considering Equation (35). It takes the form

$$P(\Theta_i,\Theta)=\frac{2\sum_{j,\Theta_i}\sum_{p}\left|\varepsilon_p^{j}\right|^2 D(j,\Theta_i,\Theta)+\frac{4J_1^2(x\sin\Theta)}{\sin^2\Theta}}{1+\int_0^{\pi} d\Theta\sin\Theta\sum_{j,\Theta_i}\sum_{p}\left(\varepsilon_p^{j}\right)^2 D(j,\Theta_i,\Theta)} \tag{40}$$

From the equation (3), the phase function of far-field scattering can also be written as

$$P^{F}(\Theta)=\frac{4\pi C_{sca}^{d}(\Theta)}{C_{sca}}=\frac{4\pi\left[C_{sca}^{d,N}(\Theta)+C_{sca}^{d,N}(\Theta)\right]}{C_{sca}^{N}+C_{sca}^{N}}$$

Note

$$C_{sca}^{N}=\omega^{N}C_{ext}^{N}=\frac{\omega^{N}C_{ext}^{N}}{2}$$

and

$$C_{sca}^{dif}=C_{ext}^{dif}=\frac{C_{ext}^{N}}{2}$$

Using these basic relations and the definition of asymmetry factor, we obtain the asymmetry factor for the far-field scattering:

$$g^{F}=\frac{1}{4\pi}\int P^{F}(\Theta)\cos\Theta d\Theta=\frac{C_{sca}^{N}g^{N}+C_{sca}^{dif}g^{dif}}{C_{sca}^{N}+C_{sca}^{dif}}=\frac{\omega^{N}g^{N}+g^{N}}{\omega^{N}+1} \tag{41}$$

Equations (21), (39-41) form the set of equations of single scattering properties for far-field scattering calculated by the geometrical-optics method.

4 Single Scattering Properties -- Calculations

Based on the formalism in section 3, numerical calculation is carried out in this section. For integration involved, if only the integral value is concerned, Gauss-Legendre quadrature method is used.

4.1 Absorption Efficiency

First we calculate the integral value of Equation (21) using Gaussian quadratures. The abscissas and weights of the Gauss-Legendre n-point quadrature formula are calculated within (-1, 1), then the actual integration interval is scaled to obtain the integral value [Davis and Rabinowitz, 1984]. Comparison of the results with exact Mie

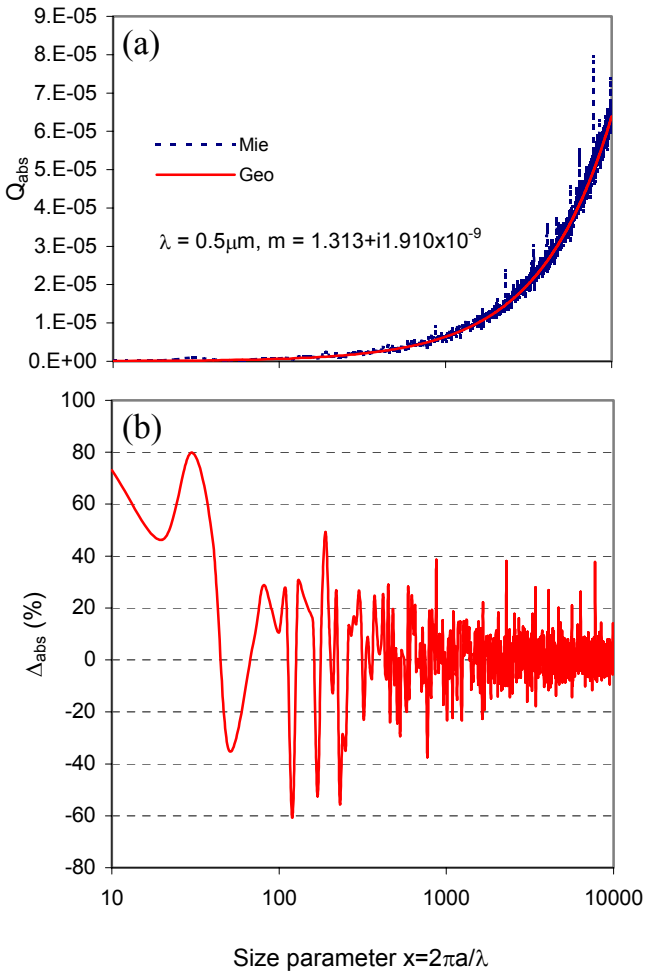

Figure 5 (a) Absorption efficiency versus size parameter x = 2πa/λ for wavelength λ = 0.5 μm corresponding to refractive index m = 1.313+i1.910×10^{-9}. Absorption efficiency is calculated using Mie scattering theory (dashed curve) and the geometrical optics method (solid line). (b) Difference factor $\Delta = \frac{Q_{abs}^{Mie} - Q_{abs}^{Geo}}{Q_{abs}^{Mie}} \times 100\%$ versus size parameter.

calculation [Wiscombe, 1980] is shown in Figure 5 and Figure 6. The variation of the absorption efficiency Q_{abs} with particle size parameter $x = 2\pi a/\lambda$ for wavelength $\lambda = 0.5$ μm is shown in Figure 5a. The dashed curve is the absorption efficiency Q_{abs} calculated using Mie theory [Wiscombe, 1980] and the solid curve is that from the geometrical optics method (GOM). To assess the deviation of the calculation of GOM from that of the Mie calculation, an absorption efficiency difference factor is defined as

$$\Delta_{abs} = \frac{Q_{abs}^{Mie} - Q_{abs}^{Geo}}{Q_{abs}^{Mie}} \times 100\% \tag{42}$$

The variation of Δ_{abs} with x for $\lambda = 0.5$ μm is shown in Figure 5b. The average difference factor for size parameter x from 10 to 10^4 is 1.46% due to many extremely narrow peaks (ripple structure). If these peaks are ignored, the difference should be smaller [Bohren and Huffman, 1983]. For large particles with x from 5000 to 10,000, the average is 1.03%. As x increases, the difference factor decreases to zero. Variation of absorption efficiency for a more absorbing band such as $\lambda = 2.0$ μm is shown in Figure 6. The results for $\lambda = 2.0$ μm is obtained using the same procedure as for $\lambda = 0.5$ μm. As the size parameter increases, Q_{abs} approaches an asymptotic value as indicated by results from both Mie calculation and the geometrical optics method (Figure 6a). The results from GOM converge to Mie results when the size parameter increases. Average Δ_{abs} versus x is shown in Figure 6b. From this figure it is readily seen that the deviation of GOM from Mie results approaches zero as $x > 4000$. Δ_{abs} decreases monotonically with size parameter when $x > 30$, with a maximum of Δ_{abs} occurring at $x \approx 30$. For $x \geq 220$, $\Delta_{abs} < 5\%$. For x from 10 to 10000, the average difference factor is 0.6%, and for large particles with x from 5000 to 10000, the average difference factor is 0.13%.

4.2 Near-field Scattering

From Equation (23), the scattering efficiency takes the form [Bohren and Huffman, 1983]

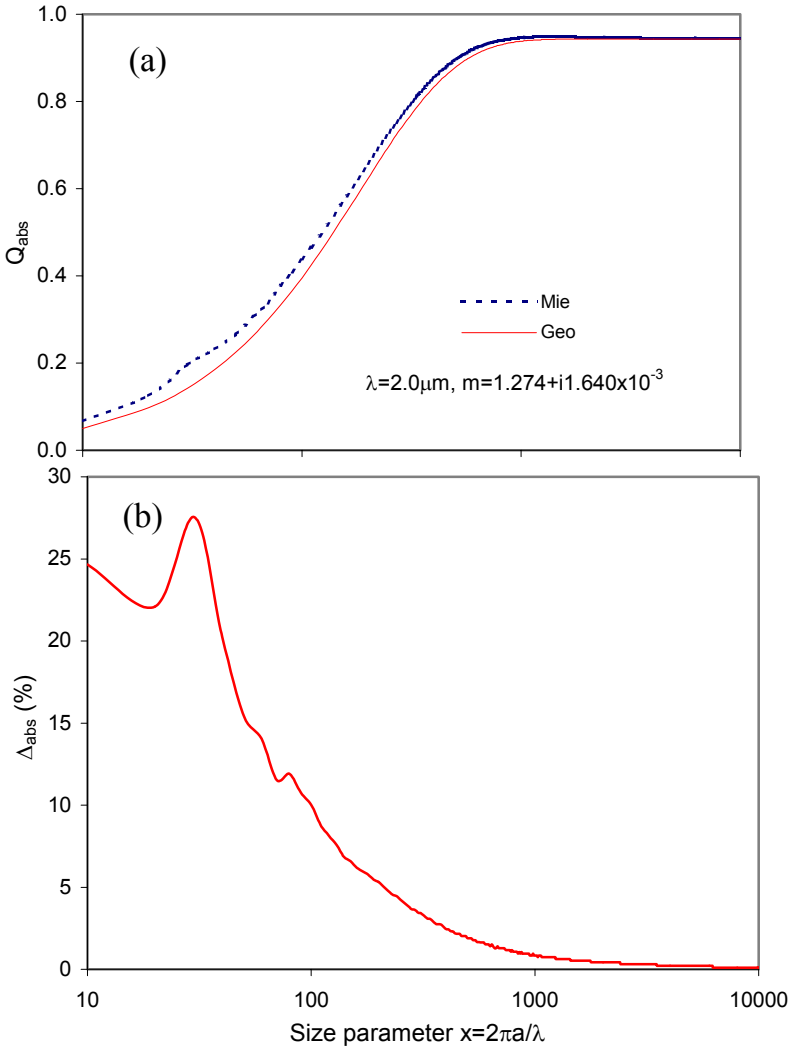

Figure 6 (a) Absorption efficiency versus size parameter x = 2πa/λ for wavelength λ = 2.0 μm corresponding to refractive index m = 1.274+i1.640×10^{-3}. Absorption efficiency is calculated using Mie scattering theory (dashed curve) and the geometrical optics method (solid line). (b) Difference factor $\Delta_{abs} = \frac{Q_{abs}^{Mie} - Q_{abs}^{Geo}}{Q_{abs}^{Mie}} \times 100\%$ versus size parameter.

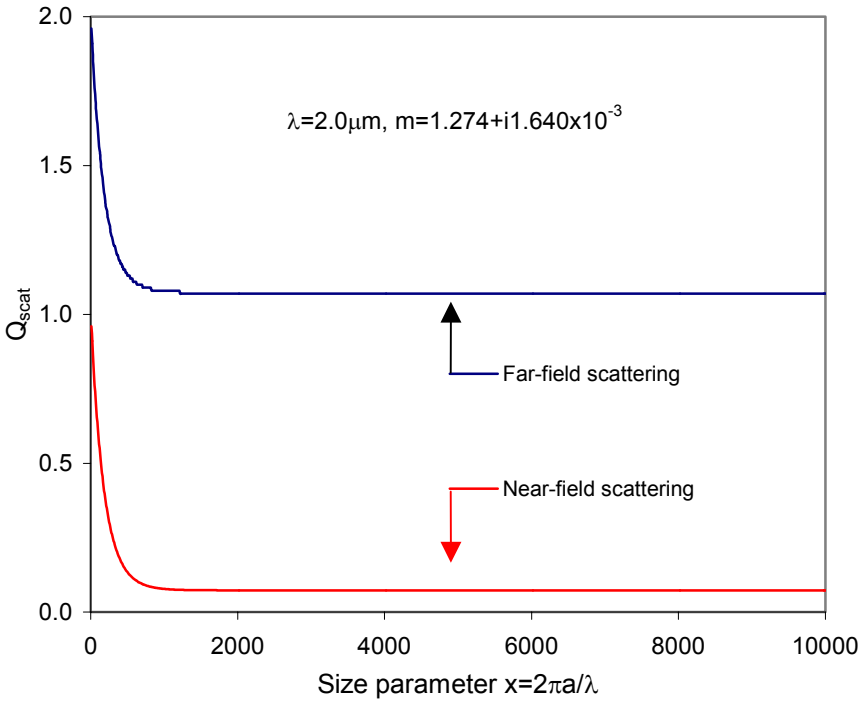

Figure 7 Near-field scattering efficiency versus size parameter x = 2πa/λ for wavelength λ = 2.0 μm. The far-field scattering efficiency for λ = 2.0 μm is also included for comparison. The difference between far-field and near-field scattering efficiencies is due only to Fraunhofer diffraction.

$$Q_{sca}^{N} = 2\int_0^1 R(\mu_i)\mu_i d\mu_i + \sum_{j=2}^{N}\int_0^1 \left[T_{//}^2(\mu_i)R_{//}^{j-2}(\mu_i) + T_{\perp}^2(\mu_i)R_{\perp}^{j-2}(\mu_i)\right] e^{-\beta\xi(j-1)}\mu_i d\mu_i \quad (43)$$

Using the same procedure as in the previous section, the integration of (43) can be obtained. For visible light, for instance λ = 0.5 μm, $Q_{sca} \approx 1.0$ for any x because the absorption is very small (Figure 5). For the near-infrared spectrum, the scattering efficiency decreases with size parameter and approaches an asymptotic value. For instance, Figure 7 shows the variation of the near-field scattering efficiency with the size parameter x = 2πa/λ for wavelength λ = 2.0 μm. The far-field scattering efficiency for λ = 2.0 μm (section 4.3) is also included for comparison. If the interference for

near-field is neglected, the difference between the far-field and near-field scattering efficiencies are exclusively due to Fraunhofer diffraction.

The phase function Equation (26a) and the asymmetry factor g can be written in the following forms when they are combined with Equation (25)

$$P(\Theta)=\frac{2\sum_{j,\Theta_i}\sum_{p}\left|\varepsilon_p^j\right|^2 D(j,\Theta_i,\Theta)}{\int_0^{\pi}\sum_{j,\Theta_i}\left(\left|\varepsilon_{//}^j\right|^2+\left|\varepsilon_{//}^j\right|^2\right)D(j,\Theta_i,\Theta)\sin\Theta d\Theta} \tag{44a}$$

$$g^N=\frac{\int_0^{\pi}\sum_{j,\Theta_i}\sum_{p}\left|\varepsilon_p^j\right|^2 D(j,\Theta_i,\Theta)\cos\Theta\sin\Theta d\Theta}{\int_0^{\pi}\sum_{j,\Theta_i}\left(\left|\varepsilon_{//}^j\right|^2+\left|\varepsilon_{\perp}^j\right|^2\right)D(j,\Theta_i,\Theta)\sin\Theta d\Theta} \tag{44b}$$

From Equation (13) we have

$$\cos\Theta=\cos\left[2(j-1)|\Theta_t|-2\Theta_i-(j-2)\pi\right] \tag{45}$$

For a given scattering angle Θ, we need to find all the sets of (j, Θ_i) that satisfy Equation (45), so that the right hand side (RHS) of Equation (45) can be evaluated. The method to obtain (j, Θ_i) is as follows: First, scan the j from 1 to N, and for each j solve Equation (45) for all possible roots of Θ_i. Then, substitute each set of (j, Θ_i) in Equation (44). Summing up all the results gives the phase function.

To solve the intractable trigonometric equation (45), let's first transform it into a polynomial equation, which is easier to solve. Setting $S=\tan\left(\frac{\Theta_i}{2}\right)\in[0,1]$, so that $\sin\Theta_i=\frac{2S}{1+S^2}$, $\cos\Theta_i=\frac{1-S^2}{1+S^2}$, Equation (45) becomes

$$f(S)=\frac{(-1)^{j-2}}{\left(1+S^2\right)^2}\left\{\left(1-6S^2+S^4\right)\cos\left[2(j-1)|\Theta_t|\right]+4S\left(1-S^2\right)\sin\left[2(j-1)|\Theta_t|\right]\right\}-\cos\Theta=0 \tag{46}$$

with

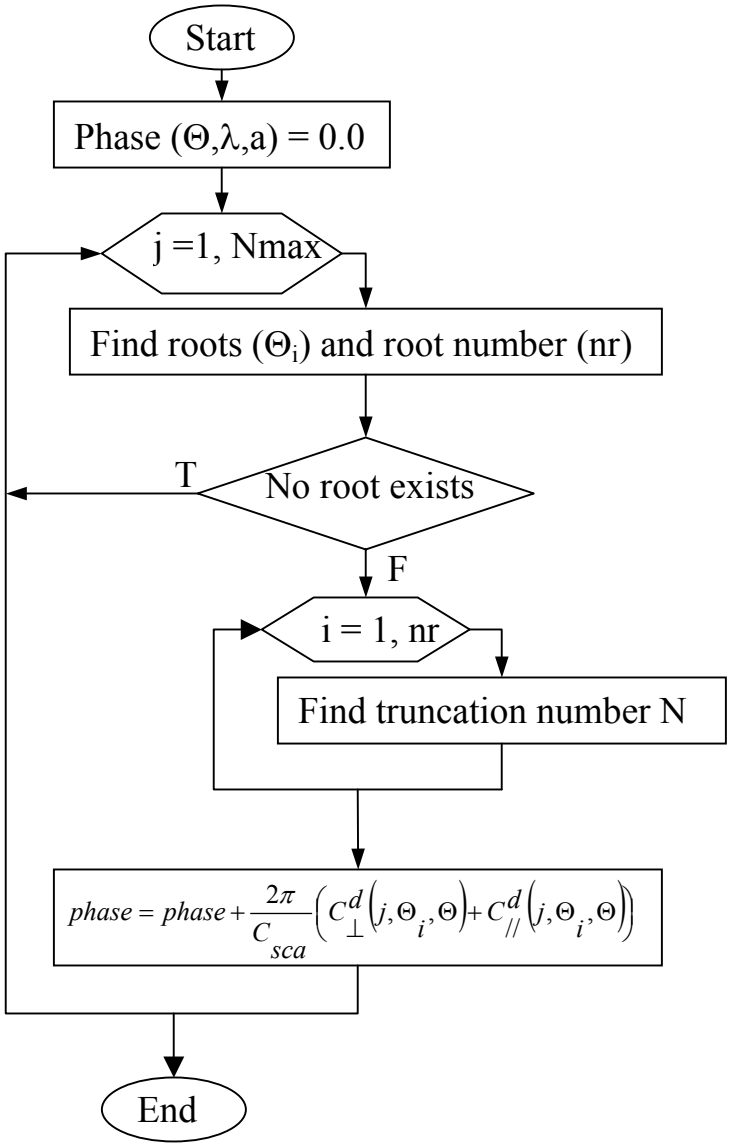

Figure 8 Flow chart for the calculation of the phase function of near-field scattering. T = True, F = False. Root-finding is based on a combination of bracketing method and a hybrid algorithm of bisection and Newton-Raphson methods. Interface number is determined by Eq. (20).

$$\Theta_t = \sin^{-1}\left(\frac{1}{\hat{m}}\frac{2S}{1+S^2}\right) = -i\ln\left[i\frac{1}{\hat{m}}\frac{2S}{1+S^2} + \sqrt{1-\left(\frac{1}{\hat{m}}\frac{2S}{1+S^2}\right)^2}\right]$$

To find the roots (S) of Equation (46) for a given scattering angle Θ, we adopt the following methods. First, we bracket the roots then utilize a hybrid algorithm of bisection and Newton-Raphson methods [Press et al., 1992]. From section 3.1 (Figure 2), we have seen that for each incident angle there exists an outgoing angle for a specific interface. But the opposite is not true. As the solution S is within [0,1], we calculate brackets for a maximum number of possible roots for n (= nmax) distinct intervals, each of which contains at most one root for each interface. Try and error method is used to find nmax. The number of interfaces is infinite if no truncation is made. The core procedure of calculating the phase function of near-field scattering is shown in Figure 8. Given the wavelength, the size (radius) of a sphere, and the scattering angle Θ, scan the interface number j to a reasonable large value jmax (larger than interface number, section 3.1). For each interface, search all the possible roots. Appropriate redirection is performed in order to include all possible sets of (j, Θ_i) in the calculation of phase function and asymmetry factor (Equation (44)). The phase function versus scattering angle of near field scattering is shown in Figure 9 for a snow grain of 1 cm. The black solid line is for wavelength λ = 0.5 μm and light solid line is for λ = 2.0 μm. For the visible light channel, the rainbows (peaks) appear at angles as shown in Table 1. However, for near infrared channels, the transmitted energy is attenuated so quickly that almost no energy is available to reach the third interface where the primary rainbow is expected to appear. Thus, the phase function for the near-infrared spectrum is much smoother than for the visible channels. To compare the results from GOMsphere code developed in this document with those from the Monte Carlo code [Nakajima et al., 1998], which deals with non-absorbing medium, Figure 10 shows the phase function for refractive index $\hat{m}$ = 1.333 + i 0.0. The data from the Monte Carlo code are taken from Table 1 of the paper by Kokhanovsky and Nakajima (1998). The results show that the agreement between the two codes is remarkably good for scattering by a non-absorbing medium.

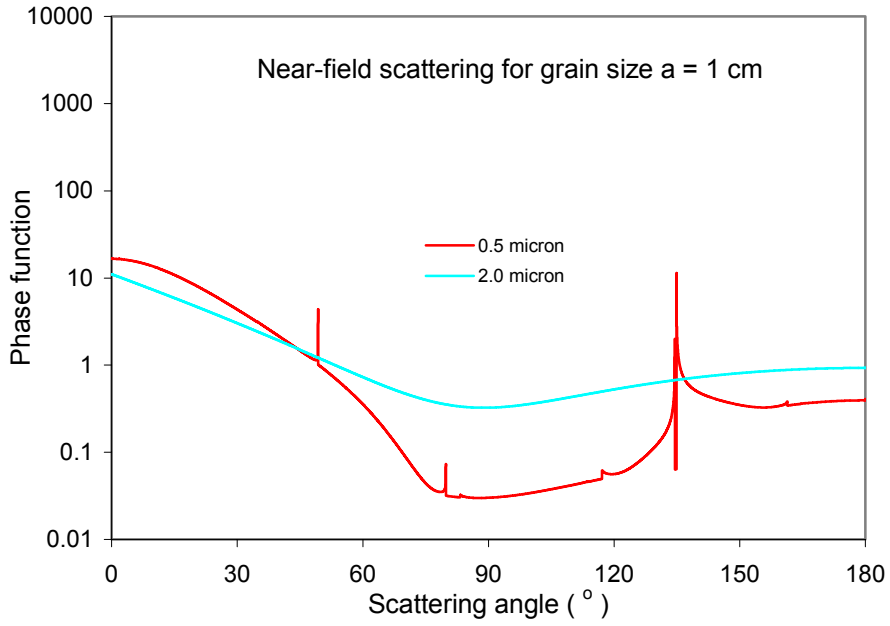

Figure 9 Phase function of near-field scattering versus scattering angle Θ for snow grains of a = 1 cm for wavelength λ = 0.5 μm and 2.0 μm. Each peak in the visible curve corresponds to the position of a rainbow.

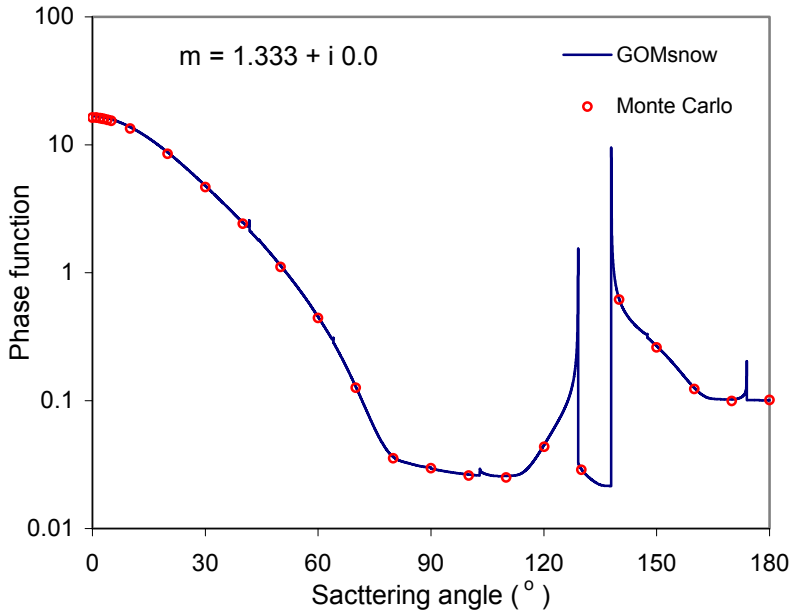

Figure 10 Comparison of the phase function calculated with GOMsphere with that from a Monte Carlo code [Kokhanovsky and Nakajima, 1998; Nakajima et al., 1998] for the non-absorbing case of $\hat{m}$ = 1.333 + i 0.0.

4.3 Far-field Scattering

The scattering efficiency for far field scattering takes the form

$$Q_{sca}^{F} = Q_{sca}^{N} + 1 \tag{47}$$

The phase function and asymmetry factor g^F are from Equations (40)-(41)

$$P(\Theta_i, \Theta) = \frac{\left[2\sum_{j,\Theta_i}\sum_{p} \left|\varepsilon_p^j\right|^2 D(j, \Theta_i, \Theta) + \frac{4J_1^2(x\sin\Theta)}{\sin^2\Theta} \right]}{1 + \int \sum \left[\left|\varepsilon_{//}^j\right|^2 + \left|\varepsilon_{\perp}^j\right|^2 \right] D(j, \Theta_i, \Theta)\sin\Theta d\Theta} \tag{48}$$

$$g^F = \frac{Q_{sca}^N g^N + g^{dif}}{Q_{sca}^N + 1} \tag{49}$$

Following the same procedure as in the previous section to find all the sets of (j, Θ_i) for a given scattering angle, scattering efficiency, asymmetry factor and phase function can be evaluated. For visible light, whose absorption in snow is negligible, the scattering efficiency is about 2.0. For the near-infrared spectrum, for instance λ = 2.0 μm, the absorption is much larger than the visible, the scattering efficiency is well below 2.0. The size parameter dependence of Q_{scat} is shown in Figure 11. When x ≥ 1300, Q_{scat} is almost constant. To compare results from GOMsphere with those from Mie scattering calculation, Figure 11a shows the Q_{scat} versus size parameter x from both GOM and Mie calculations. The inset of Figure 11a shows the results for x up to 10000. Differences between GOM and Mie are only visible at small x values. Figure 11b shows the relative deviation of GOM calculation from Mie calculation. For x ≥ 110, the relative deviation is smaller than 5%. For x ≥ 350, the relative deviation is smaller than 1%. Combined with the comparisons for other wavelengths we conclude that the scattering efficiency calculated using GOMsphere agrees well with Mie calculation for x as small as 300.

Phase functions of far field scattering are shown in Figure 12. For comparison, the phase functions of near-field scattering are also shown. Figure 12a is for λ = 0.5 μm

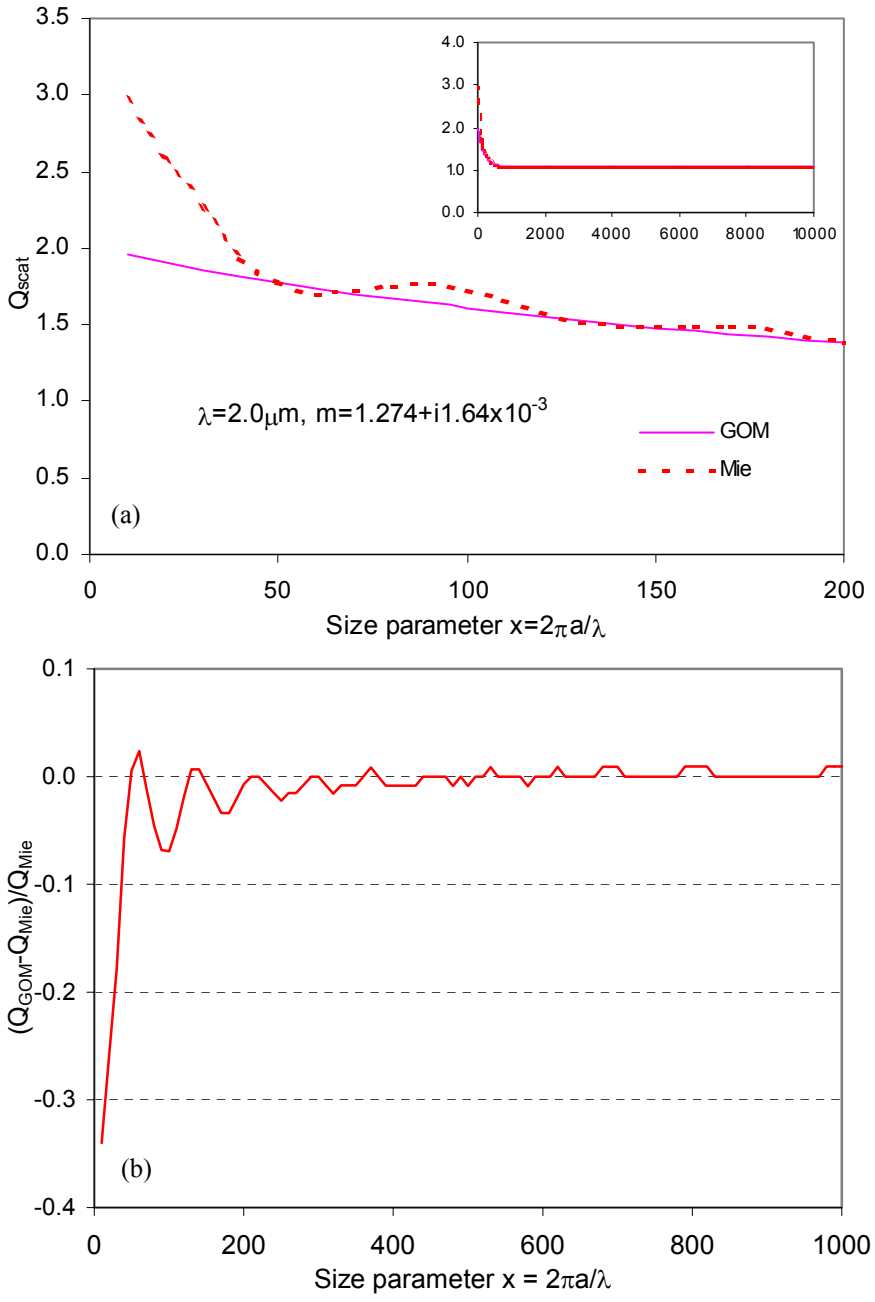

Figure 11 (a) Far-field scattering efficiency versus size parameter $x = 2\pi a/\lambda$ for wavelength $\lambda = 2.0$ μm. In the inset, the size parameter extends to 1000. The difference between Mie and GOM calculations is very small except for small size parameter (<200). (b) The deviation of the scattering coefficient calculated by GOMsphere from that by Mie0. For $x \geq 110$, the deviation is smaller than 5%.

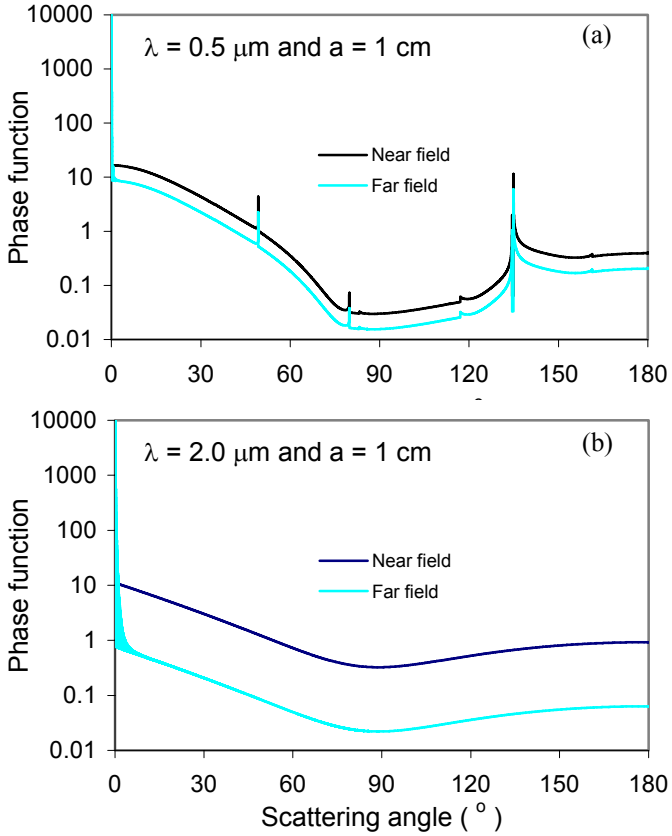

Figure 12 Phase function of far-field scattering versus scattering angle Θ for snow grains of a = 1 cm for wavelength (a) λ = 0.5 μm and (b) λ = 2.0 μm. For comparison, near-field results are also shown. Each peak appears in the visible curve corresponding to the position of the rainbow. Strong forward scattering due to Fraunhofer diffraction appears in far-field scattering phase function.

and Figure 12b is for λ = 2.0 μm. For the same wavelength, the structure of phase function for near- and far-field are similar, except in the forward scattering direction where there is a strong forward scattering for far-field scattering due to Fraunhofer diffraction. The difference between different channels for far-field scattering is similar to the case for near-field scattering. In the visible light region, multiple rainbows appear while in the near infrared region, no "rainbows" are observed for the same reason as described in section 4.2.

5 Discussion and Conclusions

The absorption efficiency, scattering efficiency and scattering phase function for both near- and far-field scattering are calculated for large snow grains on the basis of the geometrical optics method (GOM). Both the incident and scattered radiation fields are assumed to be time-harmonic. The code GOMsphere is developed to calculate these single-scattering properties. Comparison of results from GOMsphere with Mie0 indicate that the GOMsphere can be used for $x \geq 300$. Spectral dependence of these properties is obtained based on the spectral complex refractive index database of ice [Warren, 1984; Kou et al., 1993; Perovich and Govoni, 1991]. The phase function is calculated directly using a hybrid algorithm of bisection and Newton-Raphson methods [Press et al., 1992]. Comparison between GOMsphere code and a Monte Carlo code [Nakajima, 1998; Kokhanovsky and Nakajima, 1998] indicates that the agreement is remarkably good. Detailed scattering patterns can be constructed using GOMsphere. Rainbow angles appearing in the phase function agree well with analytical results [van de Hulst, 1957; Liou and Hansen, 1971]. Due to the difference of absorption or the imaginary part of the complex refractive index between the visible region and the near infrared region within the solar spectrum, rainbows mainly appear in the visible spectrum, where absorption is so weak that there exists at least one internal reflection. Rainbows seldom appear in the near-infrared spectrum, where absorption is large enough for the refracted portion of the energy to decrease to a negligible level without any internal reflection. Phase function calculations for both near- and far-field scatterings show that the angular distribution of the scattered light intensity of near-infrared channels by large snow grains is more evenly distributed than visible light.

GOMsphere was tested against a Monte Carlo code [Nakajima et al., 1998; Kokhanovsky and Nakajima, 1998]. Results from GOMsphere agrees well with Mie0 code [Wiscombe, 1979; 1980] for size parameter ≥ 200. GOMsphere and Mie0 codes can be combined to calculate single scattering properties for any wavelength from ultraviolet to microwave. The size parameter is unlimited for GOMsphere when size parameter ≥ 200. The code is computationally efficient and the computing time is almost independent

of size parameter, while for Mie0 code the size parameter is limited (< 20000) and computing-time is intensive when the size parameter is large. The calculated angular scattering patterns agree well with Mie calculation for any incident angle, rather than only good for the incident angle ≤ 60° using geometrical optics method as obtained by Glantschnig and Chen (1981). This is because the number of internal reflections truncated based on the truncation tolerance number (see section 3.1) is a dynamic parameter that depends on the incident angle, while Glantschnig and Chen's calculation was based only on N = 2.

The GOMsphere code is a computer program written in ANSI 77 standard FORTRAN to calculate the absorption coefficients, scattering coefficients and phase function for both near- and far-field scattering of unpolarized radiation by snow grains in the solar spectrum, as well as at thermal infrared and microwave wavelengths. For general purposes, the three input parameters are wavelength of the light in meters, radius of the snow grain in meters and scattering angle in radians. If only absorption and scattering coefficients are needed, only wavelength and radius of the snow grain are inputs, and the scattering angle can be set to any value. The code and this document can be downloaded from http://www.ees.nmt.edu/zhou/GOMsphere/.

ACKNOWLEDGMENTS

The research involved in this document was supported by the National Aeronautics and Space Administration under grant NAG5-6338 to the University of Alaska Fairbanks.

REFERENCES

Bager, H., 1962: Physics and Mechanics of Snow as a Material, P.8. U. S. Army Cold Region Research and Engineering Lab., Hanover, N. H., 1962.

Barber, P. W., and S. C. Hill, 1990: Light Scattering by Particles: Computational Methods, Singapore: World Scientific.

Bohren, C. F., and B. R. Barkstrom, Theory of the optical properties of snow, J. Geophys. Res., 79(30), 4527-4535, 1974.

Bohren, C. F., 1978: Scattering of electromagnetic waves by an optically active cylinder, J. Colloid Interface Sci., 66, 105-109.

Bohren, C. F. and D. R. Huffman, Absorption and Scattering of Light by Small Particles, Wiley, New York, NY (1983).

Bohren, C. F., and S. B. Singham, 1991: Backscattering by nonspherical particles: Areview of methods and suggested new approaches, J. Geophys. Res., 96, 5269-5277.

Born, M. and E. Wolf, Principles of Optics, Sixth (Corrected) Edition, 1980, Oxford, Pergamon Press, 1980, pp.808. Colbeck, S. C., 1979: Grain clusters in wet snow. J. Colloid Interface Sci., 72(no.3): 371-384.

Colbeck, S. C., 1979: Grain clusters in wet snow. J. Colloid Interface Sci., 72(no.3): 371-384.

Davis P J, P Rabinowitz, "Methods of numerical integration", Second edition, Orlando, FL: Academic Press,1984. p.481-483.

Draine, B. T., 1988: The discrete-dipole approximation and its application to interstellar graphite grains, Astrophys. J., **333**, 848-872.

Draine, B. T., and P. J. Flatau, 1994: Discrete-dipole approximation for scattering calculations*, J. Opt. Soc. America*, A11, 1491-1499.

Glantschnig, W. J., and S.-H. Chen, 1981: Light scattering from water droplets in the geometrical optics approximation, Appl. Opt., 20(14), 2499-2509.

Grenfell, T. C. and S. G. Warren, Representation of a nonspherical ice particle by a collection of independent spheres for scattering and absorption of radiation, *J. Geophys. Res., 104*, 31,697-31,709, 1999.

Hallikainen, M., and D. P. Winebrenner, The physical basis for sea ice remote sensing, in *Microwave Remote Sensing of Sea Ice, Geophys. Monogr. Ser., vol. 68*, edited by F. Carsey, pp. 29-46, AGU, Washington, D. C., 1992.

Haas, C., The seasonal cycle of ERS scatterometer signatures over perennial Antarctic sea ice and associated surface ice properties and processes, *Ann. Glaciol.*, *33*, 69-73, 2001.

Hansen, J. E., and L. D. Travis, Light scattering in planetary atmosphere, *Space Sci. Rev., 16*, 527-610, 1974.

Hecht, E., Optics, Third Edition, Addison Wesley Longman, Inc., Reading, Massachusetts, 1998.

Hu, Y. – X., and K. Stamnes, An accurate parameterization of the radiative properties of water clouds suitable for use in climate models, J. Climate, 6, 728-742, 1993.

Kokhanovsky, A. A., 1999, Optics of light scattering media: problems and solutions, Praxis Pblishing Ltd, Chichester, UK.

Kokhanovsky, A. A., and T Y Nakajima 1998: The dependence of phase functions of large transparent particles on their refractive index and shape, J. Phys. D: Appl. Phys. **31**, 1329-1335.

Kou, L., D. Labrie, and P. Chylek, 1993: Refractive indices of water and ice in the 0.65- to 2.5-μm spectral range, Appl. Opt. **32** (no.19): 3531-3540.

Liou, K. N., and J. E. Hansen, 1971: Intensity and polarization for single scattering by polydisperse spheres: A comparison of ray optics and Mie theory. *J.Atmos. Sci.* 28, 995-1004.

Liou, K.-N., and Y. Takano, Light scattering by nonspherical particles: Remote sensing and climate implications, Atmos. Res., 31, 271-298, 1994.

Massom, R. A., V. I. Lytle, A. P. Worby, and I. Allison, 1998: Winter snow cover variability on East Antarctic sea ice, J. Geophys. Res. **103**(C11): 24837-24855.

Mie, G., 1908: Beitrage zur optik truber Medien speziell kolloidaler Metallosungen, Ann. Phys., 25, 377-445.

Mishchenko, M. I., L. D. Travis, and D. W. Mackowski, 1996: "T-matrix computations of light scattering by nonspherical particles: A review", J. Quant. Spectrosc. Radiat. Transfer, **55** (no.5): 535-575.

Mishchenko, M. I., 2000: Calculation of the amplitude matrix for a nonspherical particle in a fixed orientation, Appl. Opt. **39** (no.6): 1026-1031.

Morris, K., and M. O. Jeffries, Seasonal contrasts in snow cover characteristics on Ross Sea ice floes, *Ann. Glaciol.*, *33*, 61-68, 2001.

Nakajima, T. Y. and T. Nakajima, Wide-area determination of cloud microphysical properties from NOAA AVHRR measurements for FIRE and ASTEX regions, J. Atmos. Sci., 52, 4043-4059, 1995.

Nakajima, T. Y., T. Nakajima, and A. A. Kokhanovsky, 1998: Radiative transfer through light scattering media with nonspherical large particles: direct and inverse problems, Proc. SPIE, vol. 3220, 2-12.

Nussenzveig, H. M., 1992: Diffraction Effects in Semiclassical Scattering, London: Cambridge University Press.

Papanicolaou, G. C., and R. Burridge (1975): Transport equations for the Stokes parameters from Maxwell equations in a random media, J. Math. Phys., 16, 2074-2082.

Perovich, D. K. and J. W. Govoni, 1991: Absorption coefficients of ice from 250 to 400 nm, Geophys. Res. Lett., **18**(7): 1233-1235.

Press W H , S A Teukolsky, W T Vetterling and B P Flannery,"Numerical recipes in C: the art of scientific computing", Second edition, Cambridge University Press,1992. p.350-354.

Purcell, E. M., and C. R. Pennypacker, 1973: Scattering and absorption of light by nonspherical dielectric grains, Astrophys. J., **186**, 705-714.

Rayleigh, Lord, 1871: On the light from the sky, its polarization and colour, Phil. Mag., 41, 107-120, 274-279.

Rother, T., and K. Schmidt, The discretized Mie-formalism for plane wave scattering on dielectric objects with non-separable geometries, J. Quant. Spectrosc. Radiant. Transfer, 55, 615-625, 1996.

Sturm, M., K. Morris, and R. Massom, 1998: The winter snow cover of the West Antarctic pack ice: Its spatial and temporal variability, in: *Antarctic Sea Ice: Physical*

Processes, Interactions and Variability, Antarct. Res. Ser., vol. 74, M. O. Jeffries (Ed.), pp.1-18, AGU, Washington, D.C..

van de Hulst, H. C., 1946, Thesis Utrecht, Recherches Astron. Obs. d'Utrecht, 11, part 1.

van de Hulst, H. C., 1957, Light Scattering by Small Particles, Wiley, New York, NY.

Voshchinnikov, N. V., Electromagnetic scattering by homogeneous and coated spheroids: Calculations using the separation of variables method, J. Quant. Spectrosc. Radiant. Transfer, 55, 627-636, 1996.

Warren, S. G., 1984: Optical Constants of Ice from the Ultraviolet to the Microwave. Appl. Optics, **23**: 1206-1225.

Waterman, P. C., 1971: Symmetry, unitarity, and geometry in electromagnetic scattering, Phys. Rev. **D3**: 825-839.

Wiscombe, W. J., 1979, Mie scattering calculations: Advances in technique and fast, vector-speed computer codes, NCAR Technical Note, NCAR/TN-140+STR, National Center for Atmospheric Research, Boulder, Colo..

Wiscombe, W. J., 1980, Improved Mie scattering algorithms, Appl. Opt., **19**(no.9): 1505-1509.

Wiscombe, W. J. and S. G. Warren, 1980: A model for the spectral albedo of snow. I: Pure snow, J. Atmos. Sci., **37(12)**: 2712-2733.

Yang, P., and K. N. Liou, 1996: Finite-difference time domain method for light scattering by small ice crystals in three dimensional space, J. Opt. Soc. America, **A13**, 2072-2085.